Computer Assisted Methods in Engineering and Science, **23**: 171–189, 2016.

Reducing aeration and cavitation effect in shock absorbers using fluid-structure interaction simulation

Piotr Czop[1], Jacek Gniłka[2]
[1] *AGH University of Science and Technology*
Department of Robotics and Mechatronics
al. Mickiewicza 30, 30-059 Cracow, Poland
e-mail: pczop@agh.edu.pl
[2] *Silesian University of Technology*
Institute of Theoretical and Applied Mechanics
Konarskiego 18A, 44-100 Gliwice, Poland

This paper presents a fluid-structure interaction simulation applicable for evaluating and optimizing hydraulic valve designs. A special emphasis is placed on shim stack valve commonly used in automotive and railway shock absorbers. For simplicity, the problem was effectively reduced to a two-dimensional (2D) problem. This was accomplished by introducing section-lines along which the pressure profile was computed to find and evaluate the global minimum. The global minimum was then treated as the design ranking measure. This ranking function provided a means to choose an optimal design from a set of available design variants. In the presented results, the ranking is problem-specific as it identifies and localizes low pressure zones that are the root causes of both aeration and cavitation effects. The damping force performance was experimentally evaluated for both the baseline and optimized valve design using a shock absorber level test on a servo-hydraulic test rig.

Keywords: valve system, aeration, cavitation, computational fluid dynamics, fluid-structure interactions, simulation, optimization.

1. Introduction and problem formulation

Gas pockets (aeration) and vapour cavities ("bubbles" or "voids"), which form in the hydraulic fluid due to severe operating conditions (i.e., multiple high strokes), are common problems observed in hydraulic shock absorbers. These problems in turn negatively affect vehicle handling and comfort. Gas and vapour pockets negatively influence both low- and high-frequency ride quality [1, 2]. The low-frequency effect is caused by a delay in the build-up of damping force, or equivalently, a slower than expected increase of pressure in the chambers and the hysteresis loop that produces a force-velocity response attributable to abnormal fluid compressibility, which is caused by the existence of either gas (aeration) or fluid vapour phase (cavitation) during certain stages of the stroking cycle. The high-frequency effect, which manifests itself as the presence of excessive vibrations and emission of noise [3], is caused by abrupt, catastrophic collapse of cavities entrapped in a hydraulic liquid, and is also attributed to the aeration and cavitation phenomena [4].

This paper presents the method for assessing and minimizing the risk of the aeration and cavitation effect in shim-stack relief valve systems that are commonly used in both hydraulic mono-tube and twin-tube shock absorbers. This work proposes use of an advanced fluid-structure interaction (FSI) model of a valve system assembly in the piston-rod of a twin-tube shock absorber. Since the simplified analytical approach widely presented in the literature [1, 2, 5] does not provide sufficient details to successfully perform optimization of the valve geometry, advanced simulation methods are required.

This paper is divided into five sections. Section 2 presents working principles of shock absorbers and valve systems, and Sec. 3 provides an overview of a shock absorber and its components. Section 4 introduces the methodology used to simulate structure-fluid model of a valve system. Section 5 discusses the proposed valve design optimization approach, and Sec. 6 reports the experimental results of this optimization process. The final section – Sec. 7 presents the summary of the research.

2. Working principles of shock absorber and valves

This section presents the fundamental working principles of a hydraulic shock absorber from a perspective of the combined aeration and cavitation effect and its root-causes. The hydraulic double-tube damper presented in Fig. 1 consists of a piston moving in a liquid-filled cylinder.

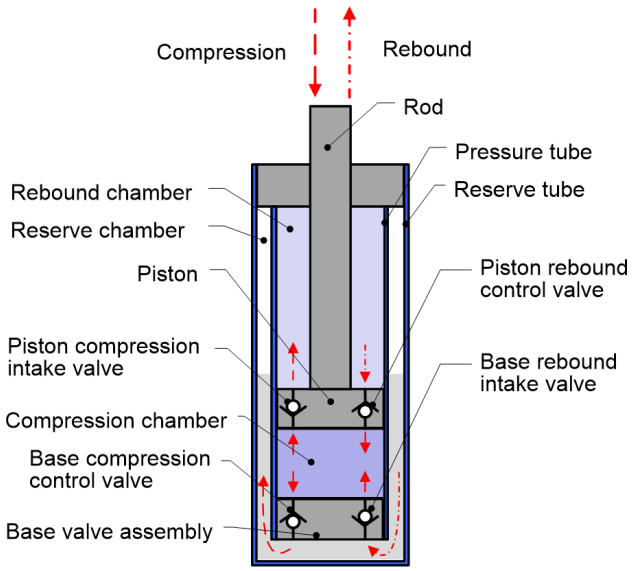

Fig. 1. Working principles of a shock absorber.

As the piston is forced to move in a cylinder (pressure tube), a pressure differential builds up across the piston and the liquid is forced to flow through valves located in the piston and the base-valve assembly. The piston divides the cylinder space into two chambers: (i) the rebound chamber (the volume of the cylinder above the piston) and (ii) the compression chamber (the volume below the piston). The action of the piston transfers liquid to and from the reserve chamber that surrounds the cylinder through the base-valve assembly located at the bottom of the compression chamber. Two types of valves are used in the shock absorber: (1) intake valves and (2) control valves. The intake valves are basically the check valves that provide only slight resistance to flow in one direction and prevent flow in the opposite direction when the pressure differential is reversed. Control valves are preloaded by a valve spring to prevent opening until a specified pressure differential has built up in the valve.

The two working phases of a hydraulic shock absorber are the compression and rebound phases. During the compression phase the rod is pushed into the damper, the compression chamber volume decreases and oil flows through the piston compression intake valve (piston intake) and the base compression control valve (base valve) accordingly, to the rebound and reserve chambers. During the rebound phase the rod is pulled out from the damper, the compression chamber volume increases, and oil flows through the piston rebound control valve (piston intake) and base rebound intake valve (base intake) accordingly to the rebound and reserve chambers. This paper considers a common type of shock absorber control valve, i.e., the clamped piston compression valve as presented in Fig. 2.

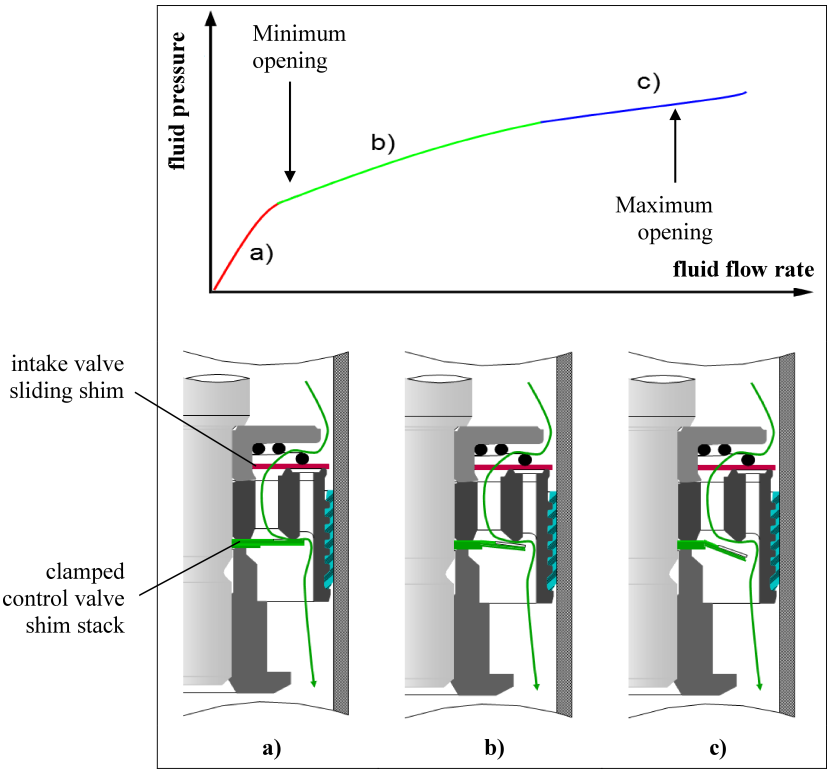

Fig. 2. Control valve characteristics and its operational regimes: a) bleed operation, b) normal operation, c) high-damping operation.

Such control valve consists of a combination of elastic shims, referred to further in the paper as a stack of shims or a shim stack. The number of shims, their diameters and thickness directly affect the operational pressure-flow characteristics of the valve system. A control valve operation is divided into three operational regimes. In the first regime, there is only a small flow through bleeds of a very small area of about 1 mm^2 in the so-called orifice shim while the stack of shims is completely closed (Fig. 2a). Therefore, the damping forces produced by the valve are very small. This regime is used while driving along a smooth road such as highway. In the second regime, the stack of shims starts to open providing a typical range of damping forces (Fig. 2b). The final operational regime corresponds to a case when the stack is fully opened and restriction is provided by the profiled channels in the piston component (Fig. 2c). This regime is used in off-road conditions or violent maneuvers on the road. This research focuses on the second and third regime. These regimes are futher referred in the work as the minimum and maximum opening of the valve system. The pressure-flow characteristics of the piston and base valves must be adjusted to meet the valve balance conditions during a compression stroke. Valve unbalance results in an effect in which the pressure in the rebound chamber becomes lower than the saturated vapour pressure during a compression stroke. This low pressure causes cavitation or gas release from oil-gas mixture (aeration) in the entire rebound chamber volume.

3. Aeration and cavitation phenomena in shock absorbers

3.1. Modeling approach

The aeration and cavitation phenomena in shock absorbers are reported by Duym et al. [1], Dixon [2], Jakubowski et al. [6], Sławik [7], Czop et al. [8], and Alonso and Comas [5]. Iyer and Yang [9] presented an analytical study on the dynamics and hydrodynamic stability of liquid-vapour mixtures in the bubble-flow range during a reciprocating motion through a horizontal channel. Their

study was used for optimizing shock absorber development. Luo and Zhang [10] provided a comprehensive review of lumped-parameter modeling methods in aeration and cavitation phenomena.

However, only distributed-parameter models provide the required component-level and design-oriented information to understand and develop a shock absorber valve system. Computational fluid dynamics (CFD) and finite element (FE) models presented in [11–13] are the most appropriate for understanding and optimizing valve systems relevant to this type of work. Beyer et al. [14] proposed a mono-tube gas-charged shock absorber model and used the FE model to obtain the valve shims' stack deflection to determine the oil flow through the valve cavity. Liang et al. [15] considered the nonlinear effects in the FE modeling of shim-type valve systems in shock absorbers. Czop et al. [16] developed and validated a line of 1D/2D FE mechanical valve shim models. Herr et al. [17] proposed a combined mathematical model of a twin-tube shock absorber, which included component models that were developed using the CFD techniques. Their component CFD analysis enabled to investigate the unique features of flow pattern, discharge coefficient, and pressure distribution inside the shock absorber components, i.e., valve systems and the rod-guide. Martins et al. [18] used contour plots of pressure and velocity obtained by using a CFD model of a shim valve system. Koren et al. [19] discussed a method for predicting high-frequency oil-flow phenomena in hydraulic shock absorbers using 2D unsteady Euler equations. Shams et al. [20] used a coupled CFD and finite element analysis (FEA) approach to predict the damping force of a piston valve used in an automotive twin-tube shock absorber. Their simulation results were also successfully verified experimentally. Yu et al. [21] used a FSI model to obtain a shock absorber performance. Guzzomi [22] presented a two-way FSI approach to predict performance of a valve system by coupling the FE model of shim stack deflection with the fluid flow CFD model. In their study, the authors used methodology similar to the methodology proposed in this study to predict valve fluid-flow characteristics. The fundamental references to fluid mechanics and coupled structure-fluid computations deployed in this paper can be found in [23, 24].

3.2. Characteristics of aeration and cavitation phenomena

The aeration phenomenon in a shock absorber is defined as a process by which gas, typically nitrogen, is circulated through, mixed with, or dissolved in oil used as the working fluid in shock absorbers. Gas is included in shock absorbers under a certain pressure and separately from the oil, to provide compressibility that compensates the rod displacement volume. Theory states [6, 10] that a liquid exposed to a soluble gas (i.e. the liquid comes into contact with the atmosphere of a gas that can dissolve in it) is in one of three forms: liquid-gas solution, liquid-gas bubble emulsion or foam.

The liquid-gas solution is prone to bubble formation when the pressure of the liquid-gas solution falls below the saturation pressure. In this state, the liquid is no longer capable of retaining all the gas in its dissolved form and cavitation bubbles therefore occur. The solubility of gas in a liquid is directly proportional to the absolute pressure above the liquid surface (Henry's law), and usually decreases with rising temperature [2]. All of the mentioned liquid-gas mixtures can be considered as liquid with pockets of gas or vapour. The dissolved gas has a significant influence on the oil mixture and thus on the shock absorber's behavior. Gas bubbles are the cause of the loss of damping force in the shock absorber. This undesirable and negative effect is observed as asymmetry of the force displacement characteristic and should be minimized.

Modeling the dynamics of gas bubble formation and transport is a very difficult task for several reasons. The most important are the difference between the time scales in which aeration processes occur (order of minutes) and the time scales of oil flow through a damper (order of seconds), the presence of uncontrollable parameters on which a bubble size depends and the bubble size itself (e.g., oil impurities and sharp edges), the re-absorption of gas from the bubbles surface, etc. The risk of aeration risk increases as the oil temperature in a shock absorber increases due to severe operation such as off-road and bumpy-road driving. However, the oil viscosity decreases reducing

the damping force effectiveness of valve systems and shock absorber. The risk becomes greater if the nitrogen gas is not separated from the oil, as it is in double-tube shock absorbers. The cavitation phenomenon occurs when oil ruptures under the influence of tensile stress, and manifests itself as a number of very small cavities in the oil [4]. The process of cavitation depends, among other things, on the purity of the liquid and the rate at which the liquid is stressed. In other words, cavitation is the formation of pockets of vapour in a liquid and it occurs when the local ambient pressure at a point in the liquid falls below its vapour pressure. As a result, the liquid undergoes a phase change to a gas, and consequently "bubbles" or, more accurately, cavities form in the liquid. The bubble growth is governed by the Rayleigh-Plesset equation [4] depending on the relative vapour-gas content and the external pressure level.

Unexpected and violent (catastrophic) collapse of cavitation or aeration bubbles results in the emission of noise as well as possible material damage to nearby solid surfaces [4]. Noise is a consequence of a large pressure (shock) wave generated during bubble implosion. This shock wave is also responsible for the occurrence of a micro-flow in the liquid [3]. The risk of cavitation during the compression stroke increases as the pressure in the rebound chamber becomes lower than the saturated vapour pressure of the oil in damper. This results in a damping force lag during the start of the next rebound stroke, since the voids must collapse first. If, during a compression stroke, the pressure in the upper pressure tube chamber becomes lower than the pressure in the reserve tube chamber, gas (nitrogen) from the reserve tube is sucked into the pressure tube trough the rod-guide seal, which results in a damping force lag during the start of the next rebound stroke. Table 1 provides an overview of the distinctive features of aeration and cavitation phenomena.

Table 1. Characterisation of aeration and cavitation effect in shock absorbers.

Description	Aeration	Cavitation
Conditions	Always present.	Oil pressure is smaller or equals the oil vapour pressure at a given temperature.
Evaluation	Phenomenon is governed by properties of the oil (solubility) and external factors (temperature and gas pressure at oil-gas contact surface).	Oil phase transition tables are required to determine the liquid/vapour saturation limits.
Quantification	Henry's equation [2].	Antoine's equation [2].
Mechanism	A result of pressure drop and/or temperature increase; gas release from the oil-gas solution in a form of bubbles.	Local pressure drop causing local 'boiling' (instantaneous evapouration).
Effect	Decrease of the bulk modulus of gas-oil mixture.	Noise due to collapsing bubbles, damage of solid elements.
Location	Entire volume of liquid in the form of oil-gas bubbles emulsion.	Locally at low pressure zones (e.g., flow restrictions).
Cause	Pressure drop in a volume of oil-gas solution, mixing and/or bubble shattering at flow restrictions.	High flow restrictions (sudden pressure drop), highly firm valves, low pressure in the reserve tube.

Cavitation and aeration occur at restrictions where potential fluid pressure energy is converted to kinetic energy, thereby increasing the fluid flow velocity and locally reducing the pressure. An engineering objective is to minimize such risk and optimize the fluid flow passage inside the valve cavity by re-designing the valve flow geometry based on the CAD model. In this respect, CFD/FSI analysis provides the required insight into the model-driven design process. The novel method to quantify the combined effect of aeration and cavitation on hydraulic shock absorber damping using experimental measurement techniques was discussed and described by Włodarczyk et al. [25].

4. Development of fluid-structure model

From an engineering application perspective, a usable hydro-mechanical valve system model should be able to reproduce the essential properties of a valve system during operation in a shock absorber. This requires a combination of two sub-models: (i) a finite element mechanical (stress/strain) model [16], and (ii) a fluid flow model. The mechanical model allows to obtain: (i) stress in shims, (ii) displacement between the orifice and valve seat, both as a function of the pressure load. The opening of a shim stack can also be expressed as a function of the outflow area vs. pressure load. If the shock absorber geometry is known, the fluid flow model presents the outlet flow rate through the valve system as a function of the pressure load. The input of the mechanical model is a pressure drop across the valve system, while the outputs are the critical stress and displacement of a shim stack over the valve seat. The input to the flow model is the pressure drop and opening displacement, while the output is the flow rate or velocity.

4.1. Modeling approach

FSI simulations use two major approaches: monolithic and partitioned. In a monolithic approach, the equations governing the flow and displacement of a structure are solved simultaneously, with a single solver. While the partitioned approach facilitates the solution of the flow equations and the structural equations in two non-coupled simulation environments. The approach deployed in this work belongs to the second approach using iteratively two independent solvers, where the obtained geometry is transferred between the two solvers.

Conversely, the FSI methods are also classified according to the purpose of the simulation as one-way, two-way, or mixed methods [26]. One-way FSI is based on the pure mapping of physical properties resulting from the analysis of a CFD model to an FE model. These two models typically do not rely on matching the meshes. The mapping of the physical properties does not include the modification of the meshes. Two-way FSI is based on the mapping performed in an iterative loop, i.e., results of the first model are mapped onto the second model and these results are mapped back onto the first model and so on until convergence is found to be satisfactory or the process is stopped manually. A two-way FSI can include modification/morphing of the mesh of one or both of the models during the mapping phase [27]. Readers interested in fluid mechanics are referred to [23, 24].

The method proposed in this paper is a modification of two-way FSI method, where deformations of a stack of shims caused by the pressure load are transferred to the CFD model for the purpose of recalculating the CFD model results in the confining geometry configuration deformed with respect to the initial one.

This method simplifies calculations and makes the process suitable for application in commercialization-driven research in which hardware and software resources are typically of limited availability and lead time for obtaining results (time-to-market) is short. The method permits estimating effort and costs during the early engineering design stage. An approximate solution obtained by simulation can become a starting point for further experimental studies using the design of experiment approach for product and process optimization.

4.2. Model reduction process

The model proposed in this paper is a two-way FSI model in which coupling between the elastic, solid structure model and flow model is performed manually by: (i) emulating the valve preloading by forces resulting from the assembly process and (ii) emulating the valve loading by forces resulting from the operating conditions. The content of this approach indicates the necessary steps to deploy a fully-fledged FSI simulation. These steps are usually run programmatically, however this section

shows partial results when an FSI simulation is performed semi-manually, that is, each major simulation step is completed by a dedicated software package, but coupling is performed manually.

Natural symmetries of the piston design geometry may be used to further reduce the computation effort necessary to simulate the model. The symmetry of holes in the solid solid allows the reduction of the model geometry by considering only 1/8 of the piston component, which results in reducing the number of FEs by a factor of 8 in comparison to the full 3D baseline model. Figure 3 shows the axes of symmetry for both sides of the piston.

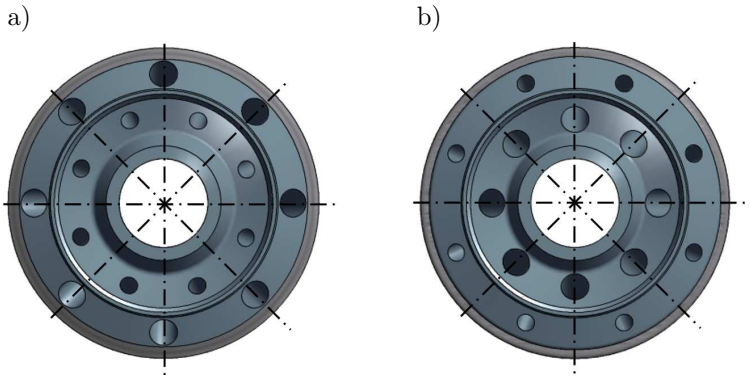

Fig. 3. Top/bottom view of the valve: a) rebound, b) compression side of the piston.

4.2.1. Preloading and simulations in the solid domain

Experience indicates that the correct determination of residual forces and stresses applied to valve components during its assembly significantly influences the accuracy obtained in subsequent simulation steps. Initial loading consist of simulating the valve assembly process by which the washer (surface 1 in Fig. 4) is moved down, while the valve seat (surfaces 2 and 3 in Fig. 4) are held fixed. Surface 1 in Fig. 4 is a head surface limiting the shims D1, D2 and D3, surface 2 determines the edge (valve seat) supporting the initially loaded shim, while surface 3 is the hub surface towards which the shims are moved after applying the preload force. Preloading step resulted in moving shims with a distance of 0.44 mm toward the valve assembly to generate the initial preload force, called the clamping force.

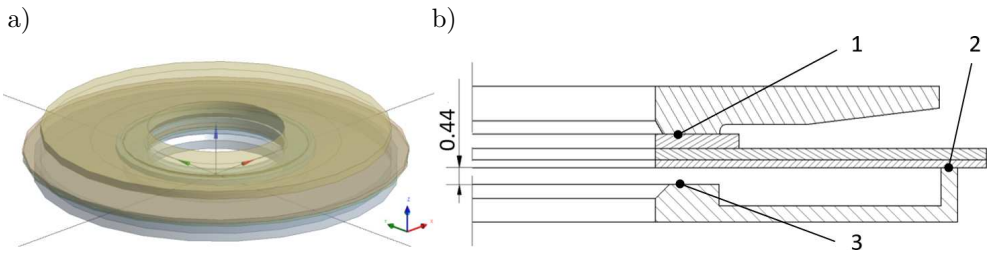

Fig. 4. CAD model of a valve: a) 3D overview, b) a cross-section with the important surfaces.

The structural model relies on 3D, non-axisymmetrical discretization of the geometry with quadratic hexahedral FEs (NASTRAN name CHEXA [28]). Thickness of each shim is decomposed onto a minimum of three to maximum five FE layers depending on the shims (D1, D2 and D3). Details are shown in Fig. 5.

Boundary conditions were defined as a rigid fixation of the valve assembly and a cylindrical fixation of the limiting shim, allowing shims D1–D3 for free rotation and axial movement. Valve assembly elements deformed during the structural simulations were not simplified.

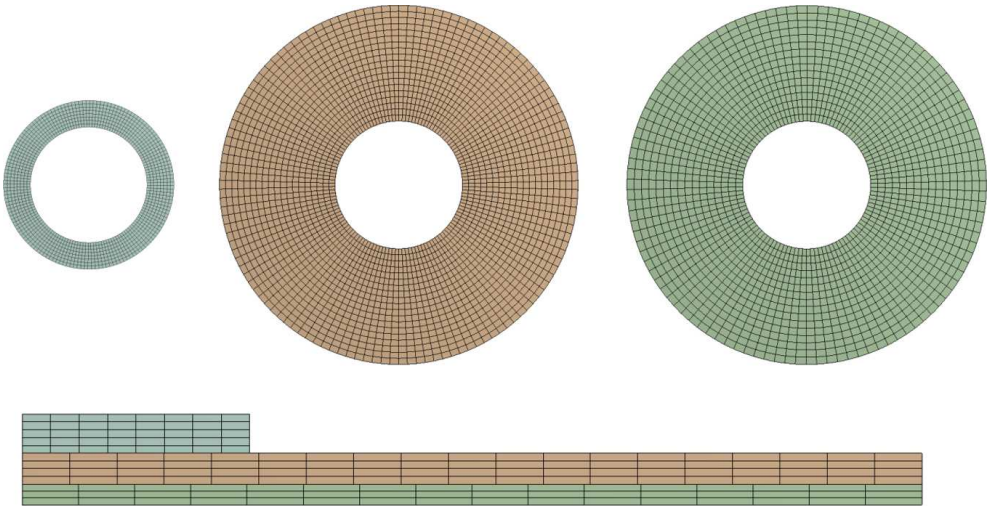

Fig. 5. Discretization of spring shims (D1, D2, D3) depending on their size (top-views and cross-section shown).

Simulation results of the reduced 3D model and results from the full 3D model are compared and summarized in Table 2. The reduced model showed stress values approximately 5% higher during the preloading step, which according to the authors, is a result acceptable from the point-of-view of model accuracy, correctness and adequacy.

Table 2. Simulation results for the baseline and reduced model.

	Units	Shim D1	Shim D2	Shim D3
Total applied displacement	mm	0.44		
Maximum von Mises stress value (full 3D model)	MPa	719	1203	861
Maximum von Mises stress value (reduced 3D model)	MPa	715	1158	897
Relative difference between the full and reduced model	%	0.56	3.75	2.02

4.2.2. Material properties

Shims are made from stainless steel springs and can withstand approximately 10^7 loading cycles inside the hydraulic shock absorber. The addition of 0.5 to 1.2% of carbon and at least 10.5% of chrome provides a high plasticity (limit) boundary above 1900 to 2200 MPa and resistance against corrosion. Properties of the hydraulic fluid are listed in Table 3.

Table 3. Fluid properties used in the flow simulation.

Parameters	Units	Values
Density	kg/m^3	840
Dynamic viscosity	$mPa \cdot s$	10 at 60°C
Working pressure range	MPa	0–20
Thermal expansion coefficient	1/°C	0.1
Viscosity indicator	1/°C	−2
Viscosity-pressure sensitivity	1/MPa	+3
Compressibility	1/MPa	+0.04
Specific thermal capacity	$kJ/(kg \cdot K)$	2.5

4.3. Simulations in the fluid domain

The CFD simulation obtained the relationship between the pressure and the flow rate of the valve system, which is of interest for the two operating points corresponding to the minimal and maximal opening of the valve (cf. Fig. 6). Geometry fed to the CFD solver was precisely the same as that determined in the preloading simulation. Simulations were conducted for the minimum opening of the stack of shims, measured as the distance between the inner edge of the valve seat and the corresponding point on the shim, equal to 0.15 mm and corresponding to a pressure range between 1.6 and 2.6 MPa with the step of 0.1 MPa. In turn, simulations for the maximal opening of 0.60 mm were performed for pressure in the range of 2.8 to 4.8 MPa with a step of 0.2 MPa.

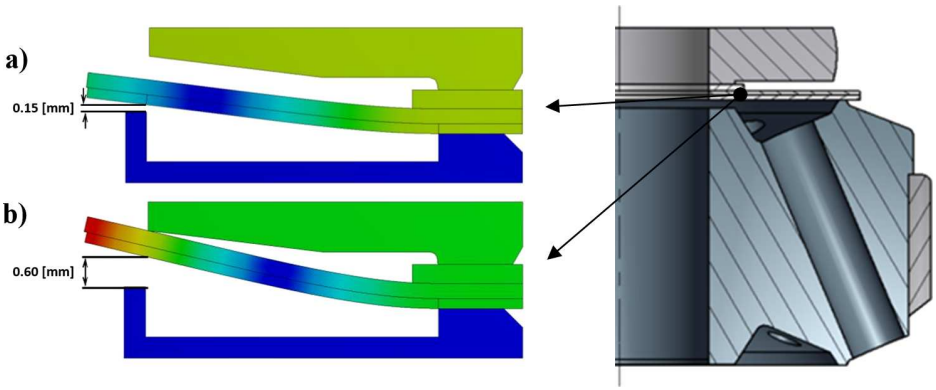

Fig. 6. Opening of the valve including the stress map of solid elements: a) bleed operation; b) high-damping operation.

Preparation of the mesh (meshing) is one of the most important factors affecting simulation accuracy and quality of simulation results. For the valve simulation described in this section, Fig. 7 shows regions (marked as A, B, C and D) where the mesh of the higher resolution was applied to investigate micro-flow perturbations, such as regions of local low pressure or whirl formation.

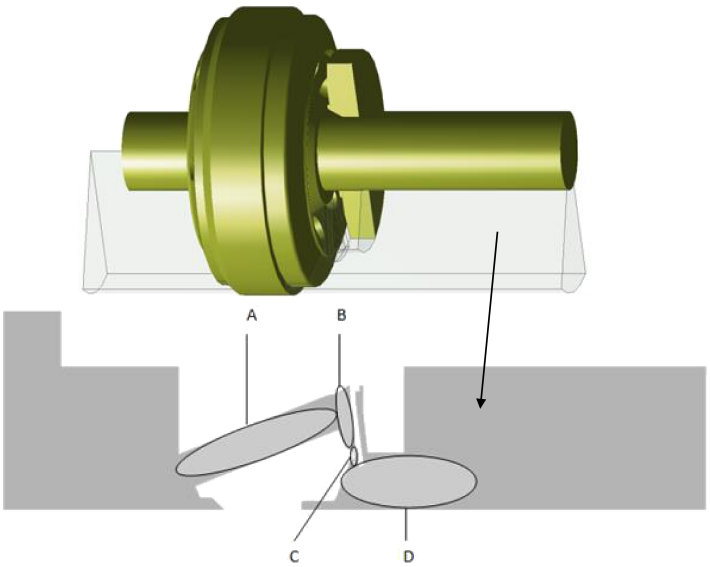

Fig. 7. Regions of the flow geometry where the high-density mesh was applied (horizontal orientation of the flow channel; the oil flows from left to right).

Region A is a narrow channel where the fluid accelerates. In region B the fluid flow is in a direct contact with the shim surface (solid), and this is a region where geometry of the channel changes

transitioning from a cylinder to a wedge. Region C is a narrow, wedge-shaped and space bounded by two solid surfaces stretched along the shim circumference. Region D, in turn, is less demanding with respect to the number of mesh elements, nevertheless it is covered by the dense mesh in order to be used by post-processing algorithms to compare the velocity field obtained through simulation to the one measured physically. It should be clear that the higher the mesh density the better the insight into the pressure or velocity field is, allowing for phenomena that deteriorate performance of the hydraulic shock absorber, such as aeration and cavitation, to be investigated in detail.

Geometry variants shown in Fig. 8 were meshed in a manner in which a balance between the accuracy and the numerical effort was achieved; respective meshes were composed of 9.5 million (large opening) and 8 million (small opening) elements. Both models incorporated a three dimensional (3D) non-axisymmetrical geometrical discretization with FE mesh based on the linear tetrahedron elements (NASTRAN name: CTETRA) [28].

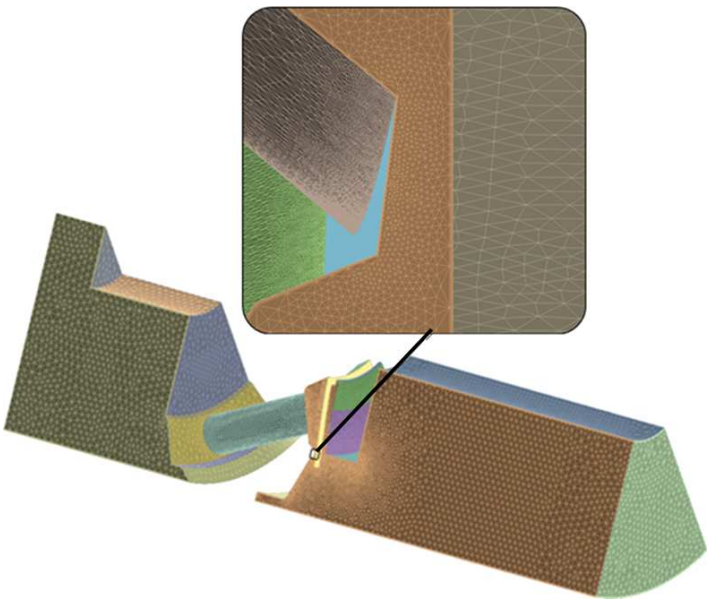

Fig. 8. The fluid model domain after the mesh creation.

Damper operation relies on viscous fluid flow through various restrictions, where the flow regime through the restrictions can be either laminar, transient or turbulent [29]. Laminar flow is evident at low excitation velocities of the piston or flow through small clearances such as piston leakage, rod sealing and guiding system, or the initial flow of the control valve [30]. When a normal and high damping valve operation regime (Fig. 2) is considered with rod velocity greater than 0.5 m/s, the turbulent flow model is applicable. The Reynolds number for piston valve restrictions can be obtained as follows [2]:

$$\mathrm{Re} = \frac{\rho u D}{\mu} = \frac{4\rho V\left(A_P - A_R\right)}{\pi \mu N d}, \tag{1}$$

where ρ is the oil density kg/m^3, V is the shock absorber's rod velocity m/s, μ is the dynamic oil viscosity Pa$\cdot$s, N is the number of channels (orifices) in the piston in the flow direction, d is the channel (orifice) diameter, and A_P and A_R are the piston area and rod area m^2, respectively. The Reynolds numbers were calculated for the piston valve including its two variants, namely six and eight channel piston designs as presented in Table 4.

The determined Reynolds number in the function of the rod velocity confirms the assumption of a turbulent flow model for piston restrictions in case of a normal and high operation regime of a damping valve. The shear stress transport (SST) model combining k–ε and k–ω models was

Table 4. Determined Reynolds number in the function of the rod velocity.

Parameters	Units	6 channel piston design			8 channel piston design		
Rod velocity	m/s	0.5	1	2	0.5	1	2
Orifice diameter	mm	2					
Rod diameter	mm	12.4					
Piston diameter	mm	30					
Reynolds number	–	2487	4975	9950	1866	3731	7462

applied due to the irregularities of the flow path and significant pressure gradients inside the valve cavity [31]. The k–ω model ensures an accurate flow modeling in flow regions in close proximity to the channel walls, while the k–ε model ensures high accuracy in the strict interior of the channel. The convergence criteria for the solver (iteration-stop criteria) were selected to be equal to $\varepsilon = 10^{-4}$ for the residual or $n = 100$ iterations. Simulation results along with interpretation and conclusions are presented in the following section.

5. Valve design optimization

The goal of primary importance in valve design optimization aimed at minimizing aeration effect is to increase the range of stable operation of hydraulic shock absorbers by improving performance of valve systems without exciting any side-effects. The valve opening should be smooth and the flow through the valve cavity should be characterized by as uniform pressure decrease along the flow path as possible and a lack of tendencies to create self-excited whirls. These requirements are achievable by smoothing sharp edges, obstacles and small cavities in the channels that induce turbulences at high velocities. Optimization of the geometry with respect to minimizing the aeration and cavitation effects should result in increased oil flow efficiency and ensure more uniform pressure distribution without the tendency to form local low-pressure regions. Valve systems used in hydraulic shock absorbers should be designed to minimize the possibility of occurrence of local low-pressure regions which contribute to the formation of gas or cavity bubbles.

It is well known from theoretical analyses and experimental investigations reported in [2, 9, 20] that aeration and cavitation in some regions in the flow defined as volumes, where the pressure value significantly falls approaching the zero reference-value, being 0.3–0.6 MPa above absolute zero pressure, achieved by the initial pressurization of the hydraulic shock absorber by the gaseous nitrogen. In consequence, the presence of aeration and cavitation causes deterioration of damping force characteristics and increases the risk of high-frequency vibrations to occur and be transferred through the suspension system to the vehicle interior resulting in the passengers perceiving a lower ride comfort, noise and harshness in the vehicle's behavior.

The analysis of the simulation results obtained for the flow through the valve cavity was performed for the minimum and maximum opening of the stack of shims as shown in Fig. 6. The flow domain has been discretized (meshed) according to the specification presented in the previous section. The section presents detailed analysis of the simulation results along with the valve optimization suggestions drawn from the CFD results.

5.1. Analysis of simulation results

Turbulent behavior of the oil inside the valve cavity is illustrated in Fig. 9 where it is noticeable that the flow is more turbulent in case of the large valve opening (bottom panel of Fig. 9) and its velocity is higher in comparison with the minimal opening of the valve (bottom panel of Fig. 9). The conclusion regarding velocity values being larger for the maximal valve opening is further

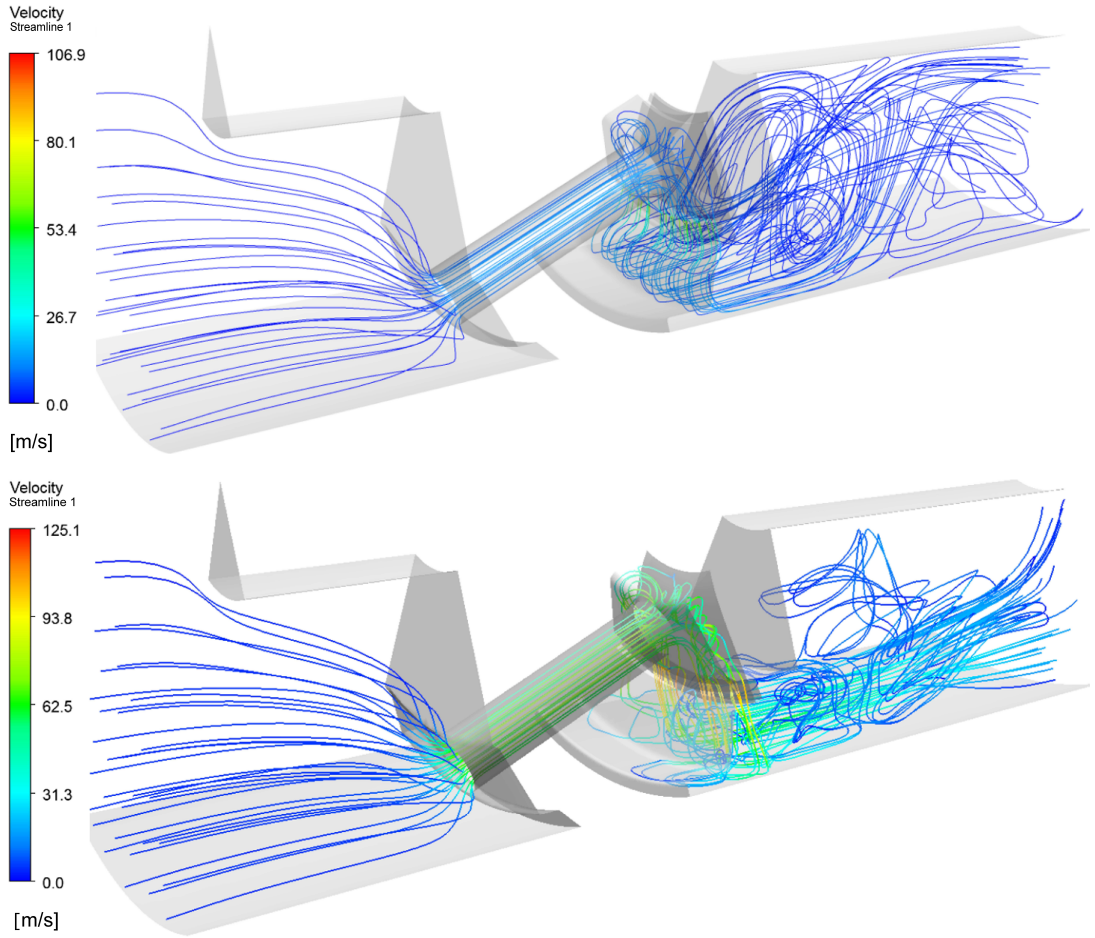

Fig. 9. Visual presentation of the fluid flow through the valve cavity with the use of velocity streams for the minimal opening (top panel) and maximal opening (bottom panel).

substantiated by analysis of velocity maps presented in Fig. 10. Visual inspection indicates the presence of significantly larger vortex structures for the maximum valve opening configuration (right panel on Fig. 11) in comparison to the minimum valve opening configuration (left panel Fig. 11). The velocity range is determined by a pressure drop across the valve assembly amounting to 2.3 and 7 MPa for the minimal opening and the maximal opening of the valve, respectively. Visual inspection of velocity and pressure maps further confirms that the pressure (potential) energy turns into flow (kinetic) energy as a high-velocity fluid jet. High-pressure gradients having a magnitude of 4 MPa at the narrowest part of the channel are visible. Value of the pressure in the valve channels initially drops below the saturated vapour pressure to subsequently return to assume a value at a level of 6 MPa.

Detailed, quantitative analysis of the pressure field is performed by plotting the pressure values along the selected lines as shown in Fig. 11 and Fig. 12. Visual inspection of Fig. 11 reveals two regions with significantly lower value of relative pressure. Presence of regions of low, or even negative, relative pressure indicates the possibility of cavitation or aeration formation. Those regions are located in the channel formed under the surface of the deflected shim and the surface to which the shim is clamped.

The first region of low pressure (pressure drop of 0.9 MPa) is formed between the external edge of the circular valve seat and the surface of the deflected shim (cf. Fig. 11), while the second region is located at the outlet of the flow channel in the piston (pressure drop of approximately 1 MPa). Pressure variation profiles along the flow direction are shown in Fig. 12 using three supporting lines shown in Fig. 11.

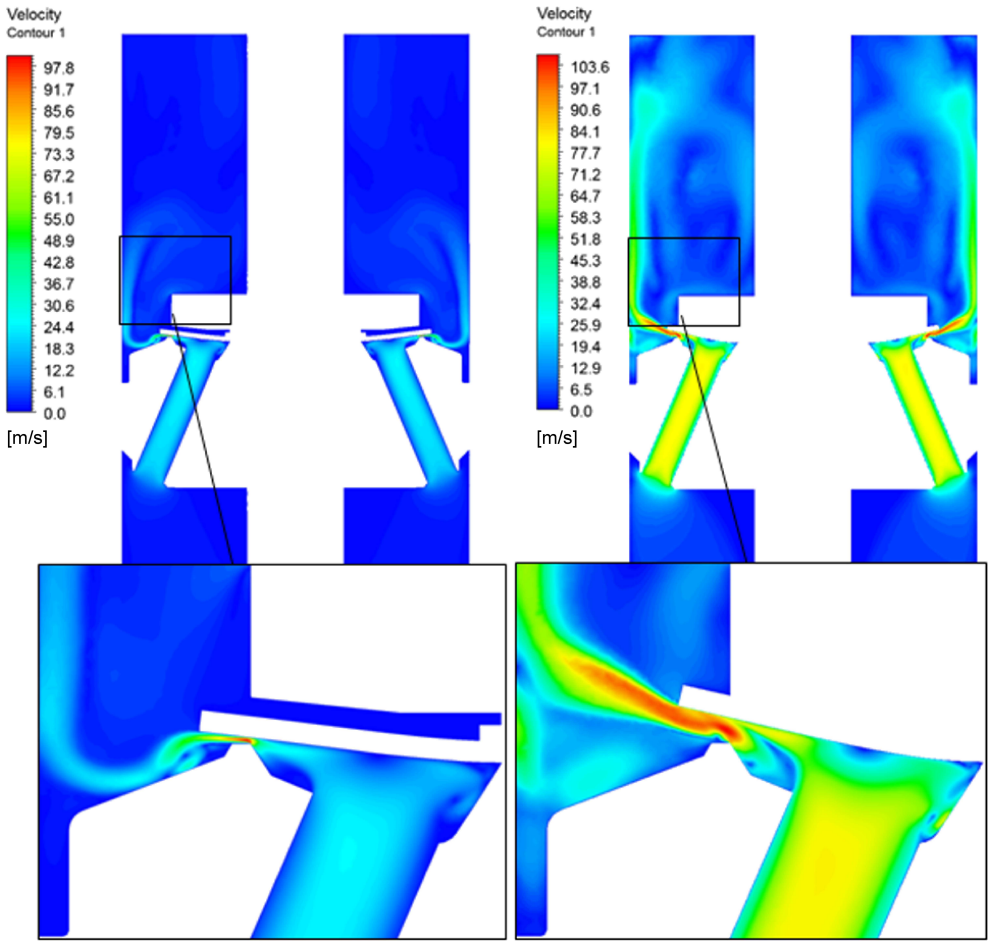

Fig. 10. Visual presentation of the fluid flow through the valve cavity with the use of velocity maps for the minimal opening (left panel) and maximal opening (right panel).

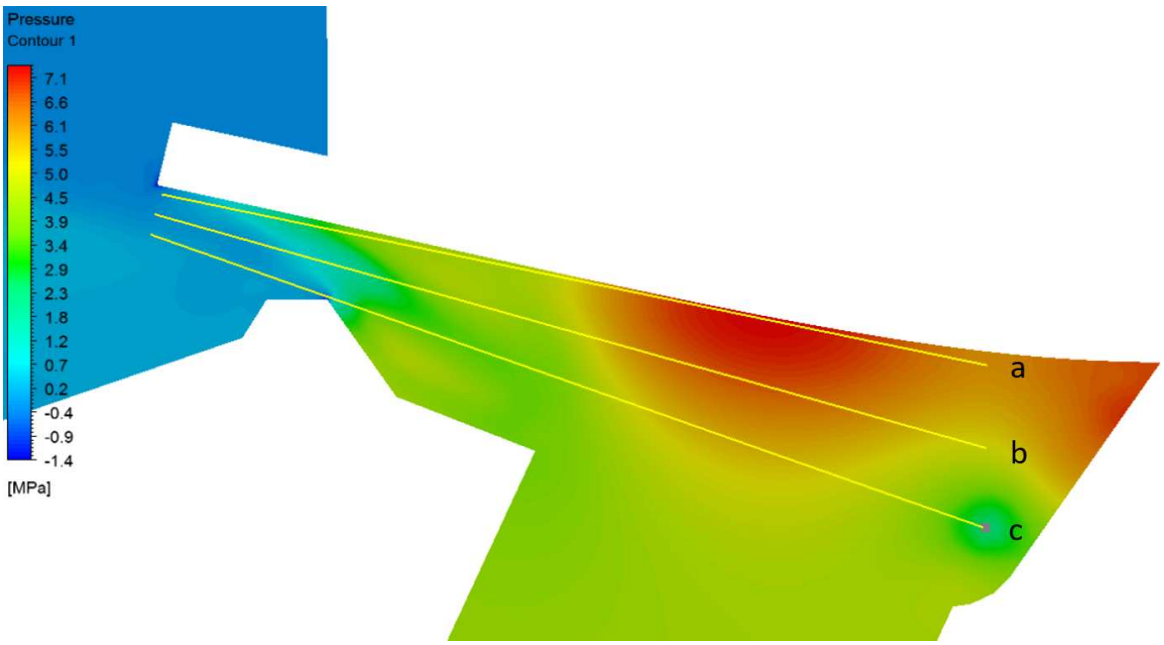

Fig. 11. Pressure profile inside the valve cavity and further over the valve seat edge (considering flow channels: a, b, c) – maximal valve opening.

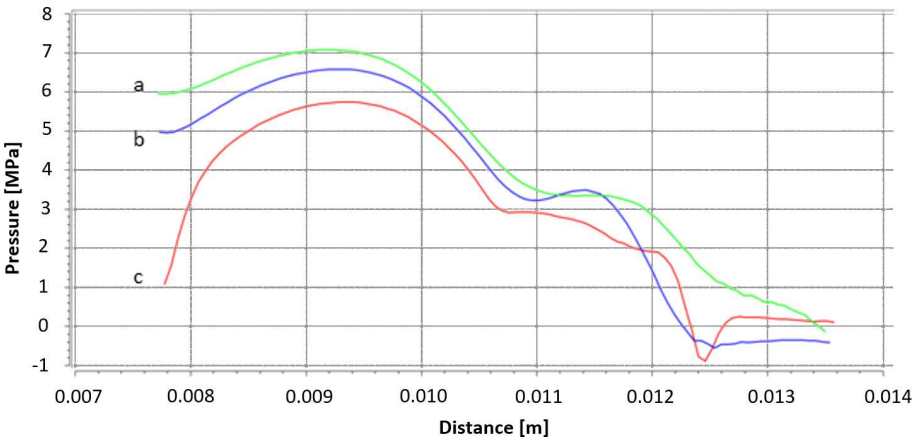

Fig. 12. Extracted pressure profiles along flow channels: a, b, c, as shown in Fig. 11.

5.2. Valve design change assessment

The authors proposed the following modification of the piston component. The valve seat and the valve cavity were shaped differently in locations indicated by markers 1 and 2 (Fig. 11). A number of proposals were verified by means of the coupled FE and CFD numerical simulations. The optimal solution was selected based on the pressure profile along the section lines and is shown in Fig. 13.

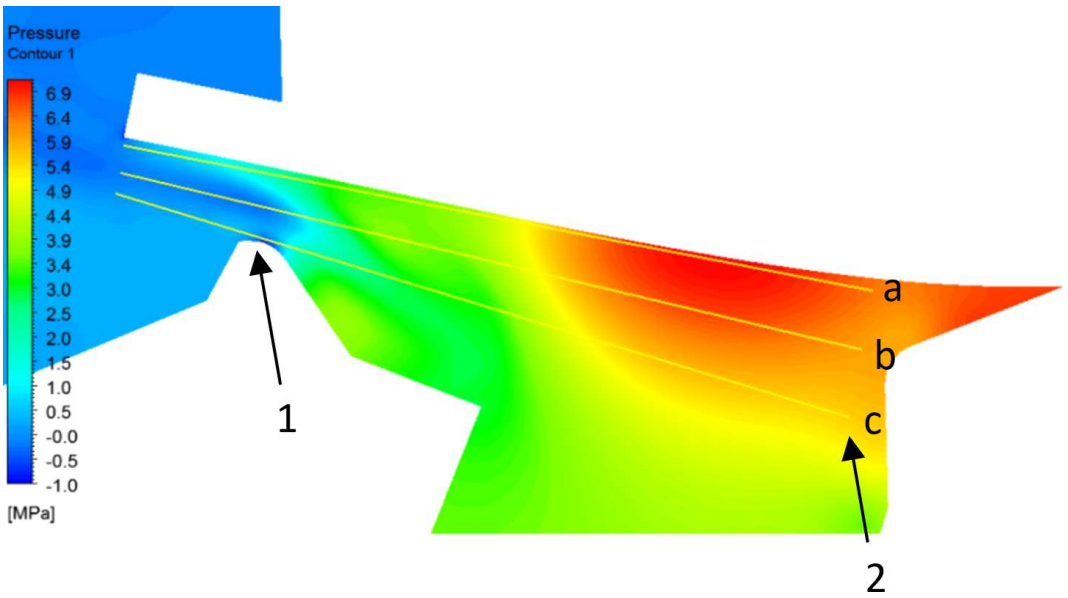

Fig. 13. Pressure profile inside the valve cavity and further over the valve seat edge (considering flow channels: a, b, c) – maximal valve opening.

The modifications introduced to create the optimal fluid flow passage geometry result in visible improvement in the second region, where the pressure increased to a level of 5.6 MPa (Fig. 14). Therefore, more uniform pressure decrease along the fluid flow channel was achieved.

Comparison of the differential pressure distribution maps in Fig. 11 and Fig. 13 indicates that a significant improvement had been achieved and was confirmed by numerical simulations. The passage geometry obtained based on numerical simulation was chosen as the best engineering solution for further experimental evaluation using a prototype shock absorber unit.

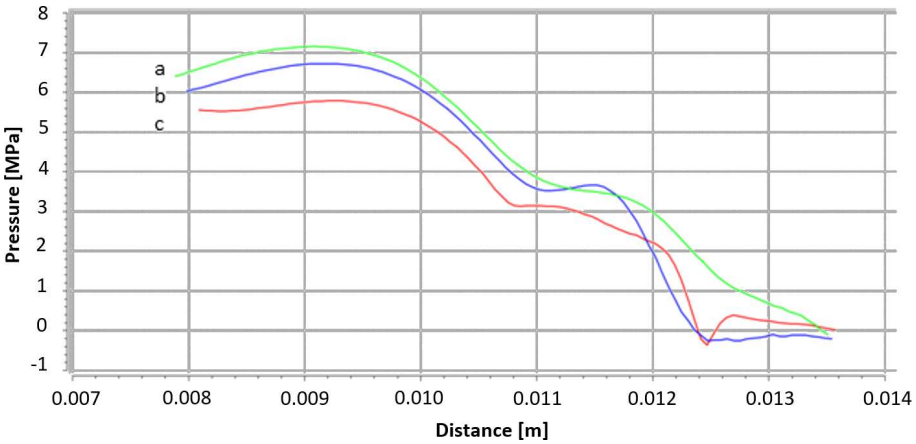

Fig. 14. Extracted pressure profiles along flow channels: a, b, c, as shown in Fig. 13 after design modification.

6. Validation results

The term "validation of a numerical model" usually refers to the process of "comparing simulation results against reality". The difficulty arises from realization that "reality" is not available for virtual measurement systems and one must be aware that only the model's ability to reproduce experimental results, either directly or indirectly via post-processing algorithms [25], may be assessed. Numerical models employed by the computational fluid mechanics are biased by an unknown level of uncertainty resulting from multiple sources such as channel geometry simplifications, meshing, fluid parameter estimation, model selection and visualization techniques used. In order to alleviate difficulties arising from this uncertainty and to obtain accurate measurements, simulation results of CFD models must be compared to and validated against results of measurements obtained from physical experiments.

6.1. Modified piston components

Shock absorber piston components are produced using sinter metal technology [32]. However, the prototype piston components are typically machined from steel. It was decided to machine the two piston components, namely the baseline and the modified version whose geometry was proposed based on the simulation results (Fig. 15). This approach ensured obtaining comparable results for both piston components.

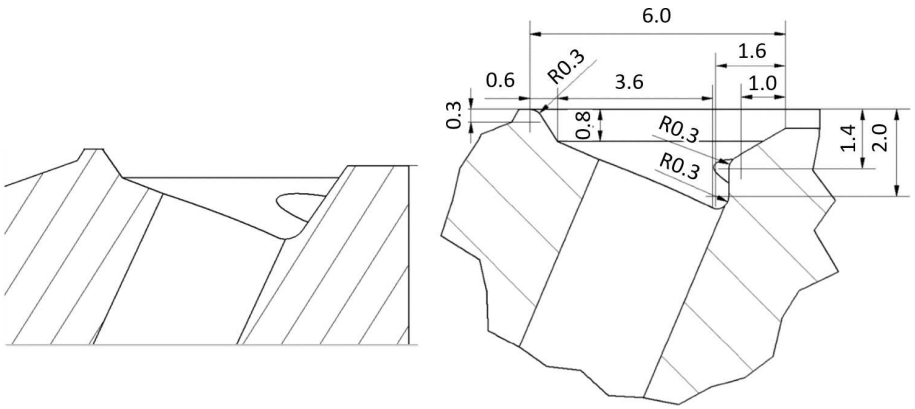

Fig. 15. Geometry of (i) the baseline (left panel) and (ii) optimized (right panel) piston component.

Availability of different piston shapes allowed assessing the influence of the geometry change on the operational characteristics of the valve, leading to selection of such a shape that would minimize the possibility of gas emission from the gas-fluid mixture as a result of passage of the fluid through low pressure and by cavitation.

6.2. Experimental validation

Experiments were performed using a Hydropuls® MSP25 servo-hydraulic test rig, equipped with an IST8000 electronic controller (Fig. 16). The test rig was used to load a hydraulic shock absorber and capture characteristics of its dynamics, i.e., the force to displacement function. Data acquisition was performed with an eight-channel ICP amplifier manufactured by LMS. The test rig was equipped with an oil supply system (the so-called servo-pack) that provided a pressure of 28 MPa at a flow-rate of 90 l/min. The actuator provided a 25 kN force applied to the damper rod and a maximum stroke of 250 mm, at a maximum achievable velocity of 3 m/s. The actuator rod was coupled to the adapter, which in turn transferred the force to a hydraulic shock absorber mounted on the test rig.

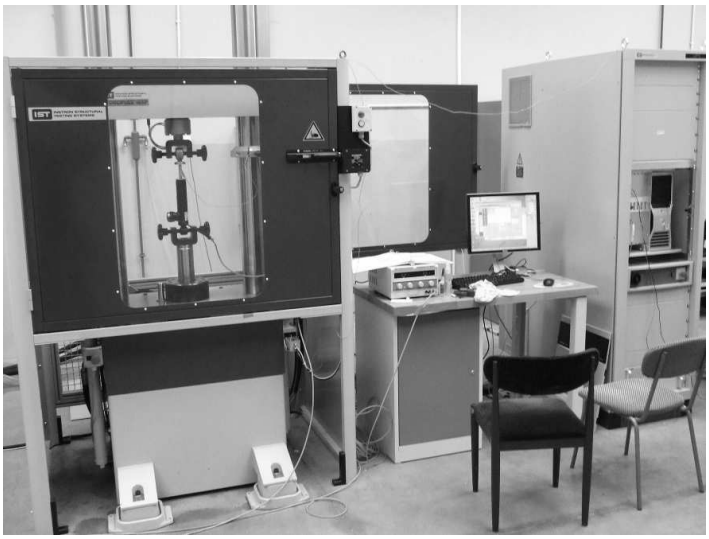

Fig. 16. A servo-hydraulic test rig used in experimental investigations.

Major components of the servo-hydraulic system were: (i) the hydraulic actuator with an integrated displacement transducer in a piston-rod assembly (IST-Schenk) and (ii) the three-stage servo-valve system. The test rig was equipped with a PID-FF controller. The feed-forward (FF) section of this controller was used to pass a portion of the command signal to the controller output through a high-pass filter to block the command mean level. Various control settings were used depending on the type of excitation signal. The excitation signal was converted to the voltage applied to the servo-valve, allowing the amount of oil supplied to the chambers of the actuator to be controlled.

6.3. Validation results

A sine-wave cycling signal of amplitude equal to 40 mm at 1.5 m/s was used to excite the prototype hydraulic shock absorbers equipped with the optimized valve system. The maximum values of the compression stroke were collected as a function of the number of combined rebound-compression and compression-rebound cycles of shock absorber operation. The test was repeated six times to

obtain the averaged results for the baseline and modified piston shape (Fig. 17). The prototype absorber unit was dissembled and assembled again after each measurement in the sequence and stored for a period of one day at room temperature ($22 \pm 2^{\circ}$C) in order to ensure the oil would be in a gas-saturated state for the next test run.

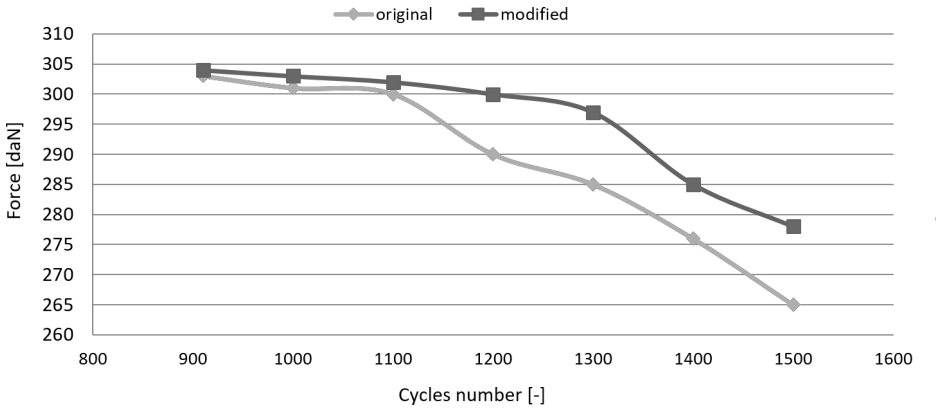

Fig. 17. Trend in decreasing the damping force for the baseline and modified valve design.

Results depicted in Fig. 17 clearly indicate that for the modified valve, the damping force starts to decrease at a considerably later stage compared to the baseline valve design. This observation confirms a lesser tendency to produce bubbles by the modified valve which, in turn, positively affects the damping force generated by the valve.

7. Summary

The aim of this work was to formulate and verify an optimal design selection method based on validated numerical models. The method presents a conceptually simple way to optimize construction design by selecting the optimal design from among a set of feasible designs. In this approach, the construction of a 'penalty function' by means of numerical optimization approach is not required, making the method easy to be implemented as an extension of existing engineering processes.

The proposed method deploys a FSI model to indicate the local pressure drop regions which are the major root cause of aeration/cavitation. The validation of the proposed geometrical changes of the valve component based on the simulation results was performed using two valve components, i.e., the baseline and the modified one. The parts were assembled in a prototype hydraulic shock absorber in order to conduct tests on a servo-hydraulic test rig.

The first step of the valve system optimization was to reduce the complexity of geometry of the valve system. This process allowed for the reduction of the full 3D baseline model to an equivalent of 1/8 the 3D model reflecting the necessary geometry, i.e., the three base surfaces. The accuracy of the simplified model differs less than 5% from the full 3D baseline model. It was evaluated that the model simplification allowed 80% of the computational time to be saved, shortening calculations to two days per single case. Thus, the optimization method can be recommended for industrial applications.

The second step was to perform a fluid-structure simulation process to analyze the simulation results, while the last step was to perform an experimental case study to verify if the proposed geometrical modification of the valve system will provide improvement in the performance of the hydraulic shock absorber cycling to avoid aeration/cavitation. The experimental investigations confirmed that the hydraulic shock absorber with the optimized valve system could work approximately 150 cycles longer in comparison with the hydraulic shock absorber equipped with the baseline valve system allowing the aeration/cavitation resistance to be increased by nearly 10%.

In respect to research on aeration and cavitation, all elements of this study's assessment set-up were verified as applicable and useful in industrial practice. Our research results are readily extendable to all valve systems for which a transparent housing can be built and installed in the particle image velocimetry (PIV) setup [33]. Additionally, mesh morphing techniques [27] and global optimization algorithms can be considered in developing a semi-automatic method to find the optimum valve design regarding numerous boundary conditions.

Findings of this work open great possibilities for extending the results shown herein as an approach to produce much more complex valve systems that should prove potentially useful in further development and the continual improvement of automotive and railway hydraulic shock absorbers.

References

[1] S.W. Duym, R. Stiens, G.V. Baron, K.G. Reybrouck. Physical modeling of the hysteretic behaviour of automotive shock absorbers. *SAE Technical Paper 970101*, 1997.

[2] J. Dixon. *The Shock Absorber Handbook*. John Wiley & Sons, 2008.

[3] S.L. Ceccio, C.E. Brennen. Observations of the dynamics and acoustics of travelling bubble cavitation. *Journal of Fluid Mechanics*, **233**: 633–660, 1991.

[4] C.E. Brennen. *Cavitation and Bubble Dynamics*. Cambridge University Press, 2013.

[5] M. Alonso, Á. Comas. Modelling a twin tube cavitating shock absorber. *Proceedings of the Institution of Mechanical Engineers, Part D: Journal of Automobile Engineering*, **220:** 1031–1040, 2006.

[6] D. Jakubowski, J. Gnilka, G. Wszołek, P. Czop. Optimization of a hydraulic damper performance with the use of fluid-structure simulation. *Advanced Materials Research*, **452–453**: 1356–1360, 2012.

[7] D. Sławik, P. Czop, A. Król, G. Wszołek. Optimization of hydraulic dampers with the use of Design For Six Sigma methodology. *Journal of Achievements in Materials and Manufacturing Engineering*, **43**(2): 676–683, 2010.

[8] P. Czop, D. Sławik, T. Wlodarczyk, M. Wojtyczka, G. Wszołek. Six Sigma methodology applied to minimizing damping lag in hydraulic shock absorbers. *Journal of Achievements in Materials and Manufacturing Engineering*, **49**: 243–250, 2011.

[9] C.O. Iyer, W.-J. Yang. Analysis on liquid-vapour bubbly-flow systems in reciprocating motion. *Journal of Fluids Engineering*, **121**(1): 185–190, 1999.

[10] F. Luo, X.L. Zhang. A review of aeration and cavitation phenomena in the hydraulic shock absorber. Advances in mechatronics, robotics and automation II. *Applied Mechanics and Materials*, **536–537**: 1369–1373, 2014.

[11] M. Borghi, M. Milani, R. Paoluzzi. Transient flow force estimation on the pilot stage of a hydraulic valve. *Proceedings of the ASME-IMECE FPST-Fluid Power Systems & Tech.*, **5**: 157–162, 1998.

[12] M. Borghi, G. Cantore, M. Milani, R. Paoluzzi. Analysis of hydraulic components using computational fluid dynamics models. *Proceedings of the Institution of Mechanical Engineers, Part C: Journal of Mechanical Engineering Science*, **212**(7): 619–629, 1998.

[13] D.N. Johnston, K.A. Edge, N.D. Vaughan. Experimental investigation of flow and force characteristics of hydraulic poppet and disc valves. *Proceedings of the Institution of Mechanical Engineers, Part A: Journal of Power and Energy*, **205**(3): 161–171, 1991.

[14] O. Beyer, B. Becher, M. Stüwing, G. Zimmermann. Measurement and simulation of the hydraulic behavior of the piston valve in a monotube shock absorber. *Proceedings of the 7th International Conference ATA*, Italy, 2002.

[15] L. Liang, X. Zhang, M. Peng, G. Qin. Non-linear characteristic simulation of hydraulic shock absorbers considering the contact of valves. *Proceedings of the 2nd International Conference on Computer Application and System Modeling*, 2012.

[16] P. Czop, D. Slawik, P. Sliwa. Static validation of a model of a disc valve system used in shock absorbers. *International Journal of Vehicle Design*, **53**(4): 317–342, 2010.

[17] F. Herr, T. Mallin, J. Lane, S. Roth. A shock absorber model using CFD analysis and Easy5, *SAE Technical Paper 1999-01-1322*, 1999.

[18] F.P. Martins, C. Siqueira, N. Spogis. Development and validation of a CFD model to investigate the oil flow in a shock absorber. *SAE Technical Paper 2005-01-4030*, 2005.

[19] B. Koren, P.F.M. Michielsen, J.W. Kars, P. Wesseling. A computational method for high-frequency oleodynamics, application to hydraulic-shock-absorber designs. *Computational Fluid Dynamics '96*, 725–731, 1996.

[20] M. Shams, R. Ebrahimi, A. Raoufi, B.J. Jafari. CFD-FEA analysis of hydraulic shock absorber valve behavior. *International Journal of Automotive Technology*, **8**(5): 615–622, 2007.

[21] Z. Yu, N. Zhang, S. Liu. Simulation analysis of dynamic nonlinear characteristics of vehicle shock absorber based on fluid-structure interaction. *Journal of Jilin University (Engineering and Technology Edition)*, **45**(1): 16–21, 2015.
[22] F.G. Guzzomi. *Investigation of Damper Valve Fluid-Structure Interaction through the Application of Experimental Visualisation Techniques*, PhD Thesis. The University of Western Australia, 2012.
[23] M.C. Potter, D.C. Wiggert, B.H. Ramadan. *Mechanics of Fluids*. Nelson Education, 2016.
[24] E.B. Wylie, V.L. Streeter, L. Suo. *Fluid Transients in Systems*. Vol. 1. Prentice Hall, Englewood Cliffs, NJ, 1993.
[25] T. Włodarczyk, P. Czop, D. Sławik, G. Wszołek. Automatic shape identification by data-driven algorithms with applications to design optimizing in hydraulics. *Journal of Transdisciplinary Systems Science*, **16**(1): 35–43, 2012.
[26] H. Lomax, T.H. Pulliam, D.W. Zingg. *Fundamentals of Computational Fluid Dynamics*. Springer Science & Business Media, 2013.
[27] A. Narayanan, A. Einstein. Morphing and parametrization technologies for CFD applications. *SAE Technical Paper 2007-01-0597*, 2007.
[28] MSC Software Corporation. *MSC Nastran User's Manual*. Santa Ana, CA, 2000.
[29] W. Borutzky, B. Barnard, J. Thoma. An orifice flow model for laminar and turbulent conditions. *Simulation Modelling Practice and Theory*, **10**: 141–152, 2002.
[30] M.S. Talbott, J. Starkey. An experimentally validated physical model of a high-performance mono-tube damper. *SAE Conference Proceedings*, pp. 505–522, 2002.
[31] F. Guzzomi, P. O'Neill, A. Tavner. Investigation of damper valve dynamics using parametric numerical methods. *16th Australasian Fluid Mechanics Conference (AFMC)*, pp. 1123–1130, 2007.
[32] B. Yalçin. Effect of porosity on the mechanical properties and wear performance of 2% copper reinforced sintered steel used in shock absorber piston production. *Journal of Materials Science & Technology*, **25**(5): 577–582, 2009.
[33] F. Guzzomi, P. O'Neill, A. Tavner. Damper valve study using particle image velocimetry. *8th International Symposium on Particle Image Velocimetry – PIV09*, pp. 288–291, 2009.